

# Digital-analog hybrid optical access integrating 56-Gbps PAM-4 signal and 5G mmWave signal by spectral null filling

**Li, Longsheng; Zhang, Xiaoling; Kong, Deming; Bi, Meihua; Jia, Shi; Hu, Weisheng; Hu, Hao**

*Published in:*
Journal of Lightwave Technology

*Link to article, DOI:*
10.1109/JLT.2020.3034381

*Publication date:*
2021

*Document Version*
Peer reviewed version

# Digital-analog hybrid optical access integrating 56-Gbps PAM-4 signal and 5G mmWave signal by spectral null filling

Longsheng Li, Xiaoling Zhang, Deming Kong, Meihua Bi, Shi Jia, Weisheng Hu, and Hao Hu

***Abstract*—A bandwidth-efficient and low-cost spectral-null-filling scheme simultaneously delivering a 56-Gbps 4-level pulse amplitude modulation (PAM-4) digital signal and a 10×400-MHz analog radio frequency (RF) signal on a single wavelength is demonstrated for high-capacity wired and wireless optical access networks. The data rate of the PAM-4 signal is consistent with the next-generation passive optical network (PON), and the PAM-4 signal inherently provides a spectral null at 28 GHz, which can be filled with the RF signal exactly at the 5G-specified millimeter wave (mmW) band. Since pulse shaping is not essential in this hybrid transmission system, a low-cost 2-bit digital-to-analog converter (DAC) is adopted for the PAM-4 signal generation. Volterra nonlinear equalizer is adopted to effectively eliminate the analog-to-digital crosstalk without reserving a frequency gap in between. The digital-analog hybrid signal is simultaneously transmitted over a 25-km standard single-mode fiber in telecom C-band and the impact of chromatic dispersion on the number of supported mmW bands is analyzed. In addition, three types of hybrid transmitters are experimentally demonstrated, among which the first-time proposed IQ-modulator-based hybrid transmitter shows the best performance.**

***Index Terms*—5G, fronthaul, digital-analog hybrid optical access, millimeter-wave radio over fiber, pulse amplitude modulation**

## I. Introduction

DRIVEN by the ever-growing broadband multimedia applications and the emerging mobile services empowered by the 5th generation mobile communication system (5G), large transmission bandwidth is needed for both wired and wireless access networks [1, 2]. Regarding the wired access network covering residential and business areas, the next-generation passive optical network (PON) with a line rate of 50 Gb/s/λ or higher is being assessed by ITU-T to fulfill the future 100-G access capacity [3]. In this cost-sensitive network, intensity modulation direct detection (IM/DD) systems with digital modulation formats such as non-return-to-zero (NRZ) and 4-level pulse amplitude modulation (PAM-4) are promising candidates [4]. As for 5G-oriented radio access network (RAN), to tackle the heavy fronthaul traffic between distributed unit (DU) and radio unit (RU) while also reducing OPEX and CAPEX, the centralized RAN architectures such as next-generation mobile fronthaul interface (NGFI) and 5G-Xhaul were proposed [5, 6]. In these networks, digital link with evolved common public radio interface (eCPRI) still plays a critical role [7-9]. Nevertheless, constrained by the massive bandwidth consumption of radio signal digitalization, it will be an enormous challenge to serve all 5G scenarios with digital fronthaul. Meanwhile, analog radio over fiber (ARoF) is superior for high bandwidth efficiency and enabling simplified base station, making it a desirable alternative for fronthauling. Given the complementation between digital and analog optical links, fixed mobile convergence (FMC) converging digital baseband and analog radio frequency (RF) signal has been extensively studied [10-12], which facilitates infrastructure sharing and wavelength saving, and enhances the link flexibility. To enable the superposition of digital and RF modulating signals at transmitter (Tx), several schemes have been proposed, such as cascaded multiple optical modulators [13, 14], parallel modulators with coherent optical carrier [15, 16], multiport modulator such as dual-drive Mach-Zehnder modulator (DD-MZM) [17,18] and IQ modulator biased at null [19], and electrical combiner [20-22]. In most of the schemes, a frequency gap is reserved and optical/electrical filter is utilized to separate the digital and RF signals at receiver (Rx), resulting in a significant waste of bandwidth. Baseband-spectrum-shaping coding is applied in [22] to create an in-band null, which accommodates the RF signal without reserving a gap yet at the cost of coding overhead and limiting RF bandwidth. Some approaches further involve polarization

Manuscript received July 23, 2020; revised 6 October, 2020; accepted 22 October 2020. Date of publication xxxxxxxxxxx; date of current version xxxxxxxxx. This work was supported in part by the National Natural Science Foundation of China under Grant 61431009, in part by the Villum Young Investigator Program (2MAC, under Grant 15401), and in part by the Natural Science Foundation of Zhejiang Province, China [No. LY20F050004]. (Corresponding author: Hao Hu.)

L. Li and W. Hu are with the State Key Laboratory of Advanced Optical Communication System and Networks, Department of Electronic Engineering, Shanghai Jiao Tong University, Shanghai 200240, China. L. Li is also with the DTU Fotonik, Technical University of Denmark, Kongens Lyngby 2800, Denmark (e-mail: lilongsheng@sjtu.edu.cn; wshu@ sjtu.edu.cn).

X. Zhang, D. Kong, S. Jia, and H. Hu are with the DTU Fotonik, Technical University of Denmark, Kongens Lyngby 2800, Denmark (e-mail: xizhan@dtu.dk, dmkon@fotonik.dtu.dk; shijai@fotonik.dtu.dk; huhao@fotonik.dtu.dk).

M. Bi is with the School of Communication Engineering, Hangzhou Dianzi University, Hangzhou, Zhejiang 310018, China (e-mail: bmhua@hdu.edu.cn).

Color versions of one or more of the figures in this article are available onlineat http://ieeexplore.ieee.org.

Digital Object Identifier xxxxxxxxxxxxxxx

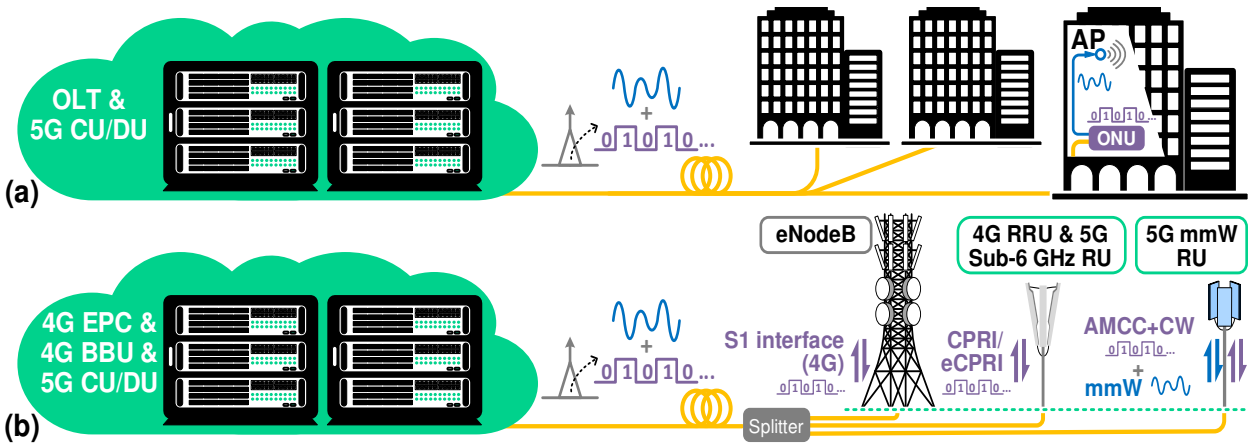


Fig. 1. Scenarios of the hybrid transmission for (a) indoor mmW enhancement, (b) co-delivery of multi-generation mobile systems. OLT: optical line terminal; CU: centralized unit; DU: distributed unit; AP: access point; ONU: optical network unit; EPC: evolved packet core; RU: radio unit; BBU: baseband unit; RRU: remote radio unit; AMCC: auxiliary management and control channel; CW: control word.

multiplexing which will complicate the system [13, 23]. In [24], a limiting amplifier is leveraged to separate signals in time domain, while the digital signal is restricted to NRZ format. Besides, in many works, the digital-analog hybrid signal is generated by a high-resolution high-sampling-rate digital-to-analog converter (DAC) [24, 25], which is costly for a practical system. Moreover, compliance with industrial standards is another challenge for implementing the hybrid transmission.

In this paper, we propose and demonstrate the simultaneous transmission of the 56-Gbps PAM-4 signal and the millimeter wave (mmW) ARoF in the downlink using spectral-null-filling (SNF) approach. With a cost-effective 2-bit DAC, the generated 56-Gbps PAM-4 signal presents a spectral null at 28 GHz, which can be filled with the RF signal exactly at 5G operating bands (24.25~29.5 GHz, [26]). Hence, the digital signal is easily compliant with the targeted speed of the next-generation PON while the bands of the integrated RF signal are 5G-specified. We demonstrate that the digital signal can be demodulated and the analog-to-digital crosstalk can be removed without reserving a frequency gap by using Volterra equalization, thereby fully utilizing the system bandwidth. Given only a single modulator is required at the Tx side, without high-resolution DAC, optical amplifier, or RU-side frequency conversion, this scheme can be cost-efficient. The selection of mmW bands in the presence of chromatic dispersion (CD) after the transmission is also investigated. Moreover, three hybrid transmitters based on directly-modulated laser (DML), MZM, and IQ modulator are comprehensively investigated. For the MZM and IQ modulator-based schemes, 8× and 10× 400-MHz 64-ary quadrature amplitude modulation (64-QAM) RF signals converged with the 56-Gbps PAM-4 signal are successfully transmitted over a 25-km standard single mode fiber (SSMF) without employing optical amplifier, respectively. To the best of our knowledge, it is the highest access capacity ever reported for IM/DD-based digital-analog hybrid transmission.

The rest of this paper is organized as follows: Section II specifies the application scenarios of the hybrid optical access. Section III details the principle of SNF and formulates the RF signal quality in the context of SNF-induced crosstalk and CD. Section IV illustrates the experimental setups and analyzes the results. Section V concludes the paper.

## II. Scenarios of Digital-Analog Hybrid-Optical Access

At present, digital-format optical interfaces play a dominant role in wired/wireless optical access networks given their simple structures, high reliability, and easy standardization. Nevertheless, to benefit the most from the centralized RAN architecture, the Option-8 functional split should be adopted in fronthaul link as specified by CPRI [27], which dramatically enlarges the bandwidth consumption owing to the digitization of the radio signal. As a contrast, the alternative ARoF not only yields better bandwidth efficiency but also enables very simple RU by moving all frequency conversion to DU, making it a superior candidate to tackle dense RU deployment and broadband air interface. Furthermore, ARoF without data queuing also features low fronthaul latency. In this work, the proposed digital-analog hybrid transmission integrating both types of interfaces on a single wavelength can satisfy the demands of multiple access services in the downlink. In Fig. 1, two typical scenarios are described. Firstly, the hybrid transmission can well support the indoor mmW access, or the in-building distributed antenna system (DAS). Limited by the high propagation loss, indoor coverage is a severe problem for 5G mmW bands. As optical infrastructures of fiber to the X (FTTX) are assembled inside or close to buildings, it can easily strengthen the mmW-band RF signal and cover indoor blind spots by overlaying the ARoF signal upon existing FTTX link and attaching the very simple RUs serving as access points (APs). In the second scenario, the hybrid link is dedicated to the mobile base stations for diverse front/mid/backhaul interfaces. As shown in Fig. 1(b), the optical signal is split into multiple copies. Legacy 4G backhaul is transmitted via the digital interface. 4G/5G traffic with high split option (eCPRI, Option 7 or higher layer), control word (CW), and auxiliary management and control channel (AMCC) should also be transmitted digitally. These types of services or data are not bandwidth-hungry and the transmission reliability has a high priority. For broadband 5G mmW access, ARoF can be a more

promising solution with high bandwidth efficiency and low latency. Considering multi-generation mobile systems sharing one base station, it is also feasible to duplicate the digital-analog hybrid signal after optical-to-electrical (O/E) conversion.

## III. Principle of Spectral Null Filling and Signal Quality Analysis

The first goal is to keep the hybrid link easily compatible with standardized wired/wireless signals in terms of data rate and modulation format. Regarding the digitized wired link, let $x(t)=\sum_{n=-\infty}^{n=\infty} a_n \delta(t-nT_s)$, where $a_n$ is the digital value mapped to the $M$-level PAM signal, $T_s$=$R^{-1}$ and $R$ is the baud rate of the PAM signal. Concerning the PAM signal with a rectangular pulse shape, its power spectral density (PSD) can be formulated as

$$\begin{aligned} S_d(f,M) &= |P(f)|^2 S_x(f) = |P(f)|^2 \mathcal{F}\{R_X(\tau)\} \\ &= |P(f)|^2 \frac{1}{T_s}\sum_{n=-\infty}^{\infty} R_n e^{-jnT_s 2\pi f} \\ &= \frac{M+1}{3(M-1)} A_d^2 \log_2 M \; T_b \,\mathrm{sinc}^2(\log_2 M \; T_b f) \end{aligned} \quad (1)$$

where "$\mathcal{F}$[*]" stands for Fourier transformation, $P(f)$ is the spectrum of the normalized rectangular pulse, $S_x(f)$ and $R_x(\tau)$ are the PSD and the autocorrelation of $x(t)$, respectively. $R_n$ is the autocorrelation of $\{a_n\}$, $T_b$=$(\log_2 M \cdot R)^{-1}$ is the bit period, $A_d$ is the signal amplitude, and $x(t)$ are bounded by $[-A_d, +A_d]$. It is observed that the PSD shows nulls at integer multiples of the baud rate. For the 56-Gbps PAM-4 and 28-Gbps NRZ, the first null appears at 28 GHz as shown in Fig. 2(a). Among all the 5G operating bands, n257, n258, and n261 fall right into this null point [26], making it convenient to realize RF signal superposition without severe interference. Note that with the raised-cosine (RC) pulse shaping instead of the rectangular one, the spectrum of PAM signal can be narrowed and sidelobes can be compressed to reduce the interference. However, the generation of an RC-shaped signal usually demands Tx-side digital signal processing (DSP) and a high-resolution DAC with a sampling rate higher than the baud rate, which are not desirable in cost-sensitive access networks. Furthermore, with the same eye-opening height, the RC-shaped PAM signal has a higher peak-to-peak value than the rectangular-shaped one, which challenges the linear modulation range especially when the modulation range is shared by both the PAM and the high-PAPR RF signal. Therefore, the rectangular-shaped PAM is adopted in this work.

The combination of the digital and RF signals can be realized by using multiple modulators, a multiport modulator, or an electrical combiner in the transmitter. At the receiver, the digital and RF signals are mixed together after the photodetector (PD), and signal separation should be realized in electrical domain. To extract the analog RF signal from the received signal of the photodetector, a band-pass filter working at mmW band is needed. In addition, other RF components such as power amplifier and antenna are often designed with a band-pass

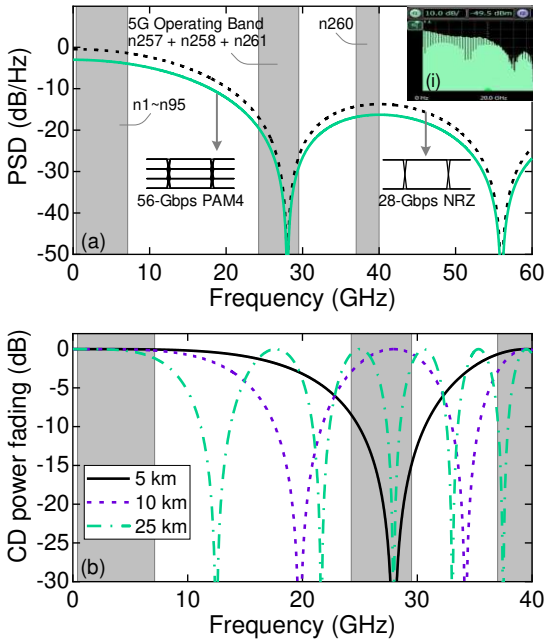


Fig. 2. (a) Spectrum of rectangular-pulse-shaped 28-Gbaud PAM-4/NRZ signal alongside with 5G wireless Operating Band, (i) 28-Gbaud PAM-4 generated by DAC (SHF 613A), (b) chromatic dispersion (CD)-induced power fading with direct detection.

response which will also contribute to the filtering. On the other hand, extracting and demodulating PAM signal from the received signal is more straightforward. In the forthcoming PON systems, Rx-side digital equalizer such as feed forward equalization (FFE) and Volterra equalizer will be employed to enhance the signal quality, which can also filter out the overlapped RF signal in the high-frequency region. This bonus of equalization is demonstrated in the following experiment.

The signal quality of the RF signal after the hybrid transmission is evaluated using error vector magnitude (EVM). With regard to C-band transmission, the RF signal impairment mainly comes from the digital-to-analog crosstalk $S_d(f,M)$ and the CD-induced power fading noted as $H_{cd}(f)$. Figure 2 (b) depicts the power fading after the transmission of different fiber length with the dispersion parameter $D$=16 ps/km/nm. Unfortunately, for the 5-km and 25-km transmission, one notch falls exactly into the mmW frequency range, making the corresponding bands unusable. To completely overcome this issue, the digital-analog hybrid transmission can be deployed in O-band. The noise at the receiver is assumed to be additive Gaussian white noise with a power density of $N_w$. The mmW-band RF signal is an orthogonal frequency division multiplexing (OFDM) signal with a total bandwidth of $B$. The RF signal is clipped to a fixed peak to average power ratio (PAPR) $R_{papr}$. Given the samples of the RF signal approximate Normal Distribution ~$N(0, \sigma^2)$, with $R_{papr}$ set to 11 dB, signal samples in $[-3.5\sigma, 3.5\sigma]$ can be covered, so that the clipping noise is negligible. Considering the SNF achieved by DD-MZM or electrical combiner, PAM and RF modulating signal should share the linear modulation depth of the modulator denoted by $[-A_0, +A_0]$. Therefore, the signal-to-noise ratio (SNR) of the RF signal after PD detection is

This article has been accepted for publication in a future issue of this journal, but has not been fully edited. Content may change prior to final publication. Citation information: DOI 10.1109/JLT.2020.3034381, Journal of Lightwave Technology



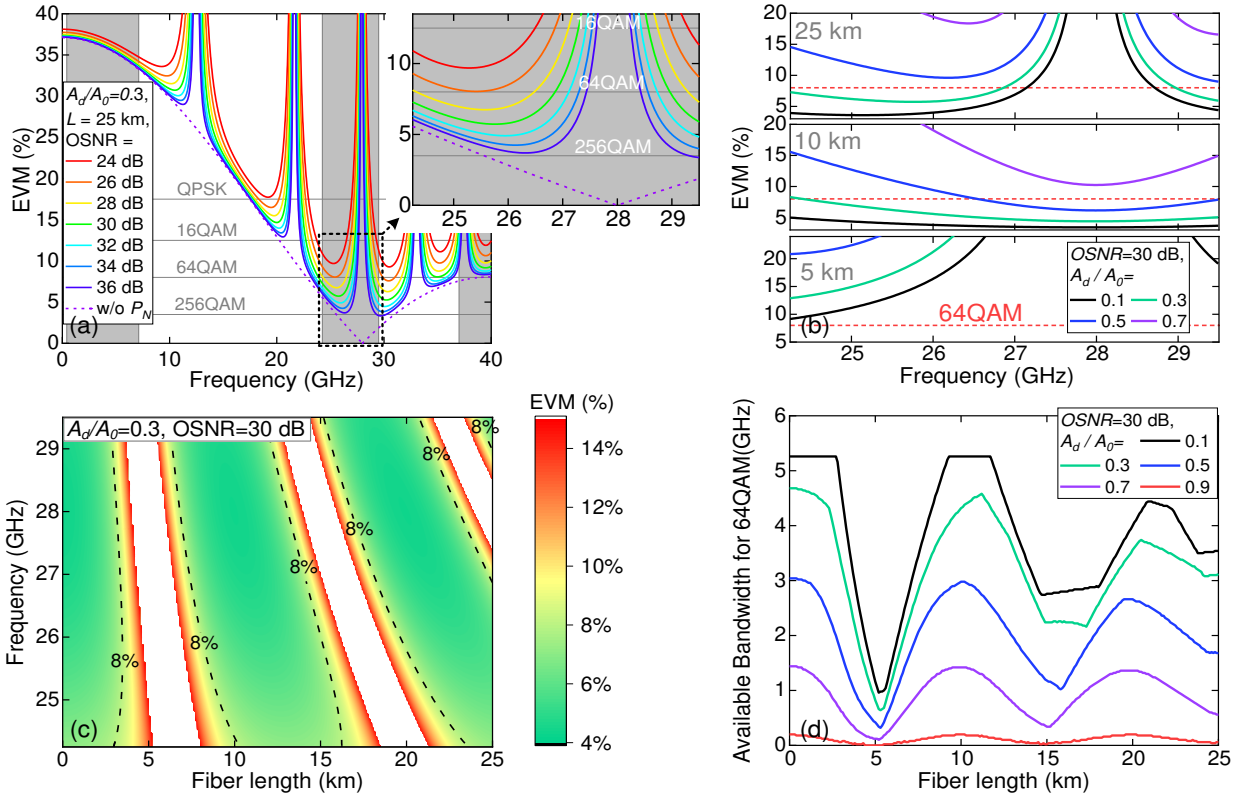


Fig. 3. (a) EVM overview of RF signal in the SNF system, (b) EVM performance under different hybrid ratios, (c) EVM with respect to frequency and fiber length, (d) available bandwidth for 64QAM. SNF: spectral-null-filling. $A_d$: amplitude of the digital signal, $A_0$: amplitude of the digital-analog hybrid signal.

$$SNR_{rf}\left(f, A_d, B, L, N_w\right) = \frac{H_{rf}(f)H_{cd}(f)S_{rf}(f)}{H_d(f)H_{cd}(f)S_d(f,M)+N_w}$$
$$= \frac{(A_0 - A_d)^2 R_{papr}^{-1} B^{-1}}{H_{rf}(f)^{-1}H_d(f)S_d(f,M) + H_{rf}(f)^{-1}\cos^{-2}\left(\frac{D\lambda^2 L}{4\pi c}(2\pi f)^2\right)N_w} \quad (2)$$

where $H_{rf}(f)$ and $H_d(f)$ represent the channel power response of the entire ARoF link and the entire PAM link, respectively, but not including CD effect. $S_{rf}(f)=(A_0\text{-}A_d)^2 R_{papr}^{-1} B^{-1}$ is the PSD of transmitted RF signal which is uniformly distributed over the total RF bandwidth $B$, and the RF band could be discontinuous. $\lambda$ is the wavelength set to 1550 nm, $L$ is the fiber length, and $c$ is the speed of light. Note that the difference between $H_{rf}(f)$ and $H_d(f)$ is mainly caused by the hardware before the SNF combination, and system nonlinearity is neglected. Since $H_{rf}(f)$ and $H_d(f)$ vary with the performance of actual components and are not the major concern, they are both normalized in this analysis. As a practical broadband link usually has a low-pass characteristic, $H_d(f)$ has strong power fading in high frequency, which will benefit the RF signal since the digital-to-analog crosstalk is reduced. Root mean square (RMS) EVM in percentage is used for signal quality evaluation, which is converted from SNR in dB by $EVM_{rms}= 10^{-SNR/20}\times 100\%$.

To comprehensively evaluate the performance of the RF signal, we investigate the EVM and the bandwidth $B$ in relation to the hybrid ratio, fiber length, and optical signal to noise ratio (OSNR). The hybrid ratio is represented by $A_d/A_0$. With a larger hybrid ratio, higher modulation depth or signal power is assigned to the digital signal. The OSNR used here is defined as $A_0^2/P_N$, where $P_N$ is the noise power spread over the PD bandwidth $B_{pd}$ which is set to 40 GHz. This definition is more accurate than the signal-over-noise power ratio since the signal power can vary with the hybrid ratio. With this definition, the noise power density $N_w$ is calculated as $P_N/B_{pd}=A_0^2 OSNR^{-1} B_{pd}^{-1}$. Figure 3 (a) shows the EVM performance with respect to the RF frequency for the cases of 24~36-dB OSNR, $B$=3 GHz, $A_d/A_0$=0.3, and $L$=25 km. The 3GPP-specified EVM thresholds are 17.5%, 12.5%, 8% and 3.5% for 4, 16, 64, and 256-QAM respectively. For the noise-free (infinite OSNR) case indicated by the dashed line, the signal quality is only determined by the digital-to-analog crosstalk. Taking into account the available OSNR after the transmission, the EVM is degraded at ~28 GHz owing to the CD fading. Figure 3 (b) shows the EVM in detail after the 5,10, and 25-km fiber transmission with an OSNR of 30 dB. It can be seen from this result that CD is the main limitation when selecting the working RF bands. Figure 3 (c) gives a more detailed look at the EVM with respect to the RF frequency and the transmission distance. The results above are all given with RF bandwidth $B$=3 GHz. By adjusting $B$, the PSD of the RF signal can be adaptive to the link performance. The maximum available $B_0$ for 64-QAM can be quantified by solving the following equation

$$\int_{24.25\times10^9}^{29.5\times10^9} \mathbb{H}\left[8\% - EVM_{rf}\left(f, A_d, B_0, L, N_W\right)\right]df = B_0 \quad (3)$$

where $EVM_{rf}$ can be calculated from $SNR_{rf}$, and "$\mathbb{H}$ [*]" represents unit step function, namely $\mathbb{H}[x]$=0 for $x$<0, and 1 for $x\geq$0. Figure 3 (d) gives the result of the available bandwidth,

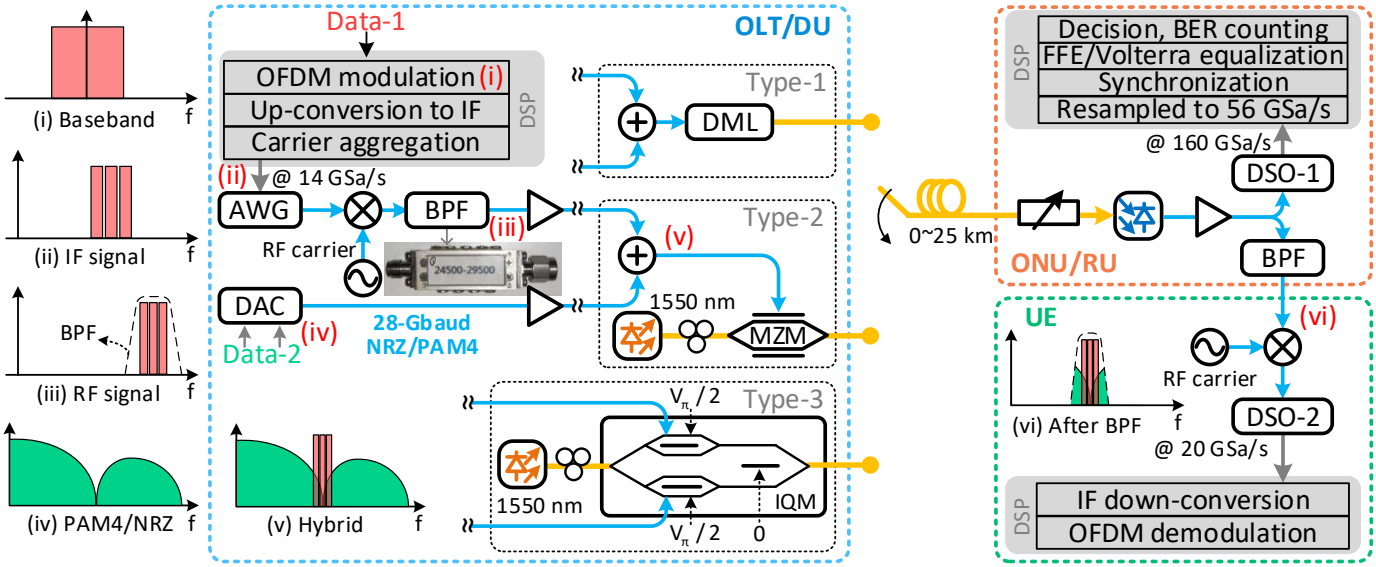


Fig. 4. (a) Experimental setup of the hybrid transmission system with three types of transmitters: DML, MZM and IQ modulator, (i)-(vi) signal spectra. AWG: arbitrary waveform generator; DAC: digital-to-analog converter; BPF: band-pass filter; DML: directly modulated laser; MZM: Mach-Zehnder modulator; IQM: IQ modulator; PD: photodiode; DSO: digital storage oscilloscope.

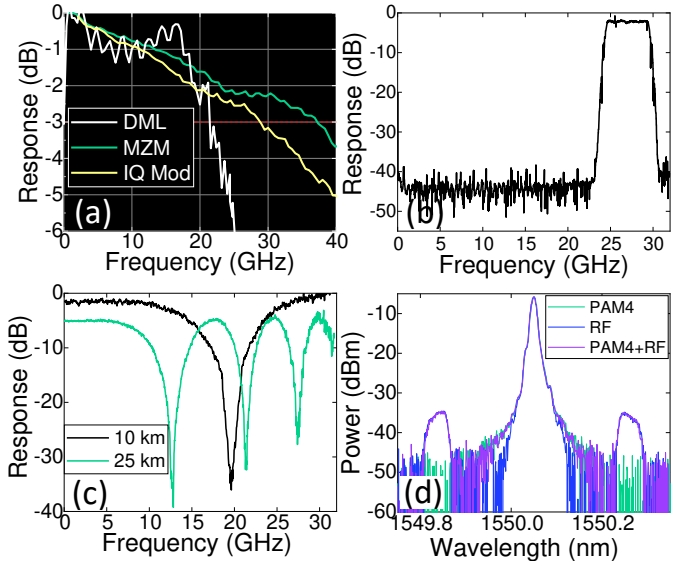


Fig. 5. Frequency response of (a) three types of optical modulators, (b) BPF, and (c) chromatic dispersion; (d) optical spectra.

indicating that the bandwidth varies dramatically with fiber length.

## IV. Experimental Setups and Result Analysis

### A. Experimental setup

The experimental setup of the hybrid transmission system is shown in Fig. 4. To evaluate the link capacity for different cost demands, three types of hybrid structures based on DML, single-drive MZM (SD-MZM), and IQ modulator are investigated, respectively. The power response of the three modulators is shown in Fig. 5(a).

The hybrid access system works as follows. The 3GPP-compliant OFDM baseband signals are generated with 120-kHz subcarrier spacing and 400-MHz bandwidth, which is the largest bandwidth that can be assigned to a single component carrier (CC). Multiple complex baseband signals are then upconverted to 400-MHz-spaced intermediate frequencies (IFs) and aggregated together. The waveform of the aggregated signal is clipped to a fixed PAPR of 13 dB and then generated by an arbitrary waveform generator (AWG, Keysight M8195A) at 14 GSa/s sampling rate (AWG is configured with 4× sampling rate divide). Note that the required sampling rate can be much lower in practical, given that the DAC only generates baseband signal and up-conversion is implemented by the following hardware. The aggregated IF signal is mixed with the RF carrier and then up-converted to the 5G mmW band. The RF carrier can be adjusted to convert the IF signal to the targeted RF band, with each band containing one CC. Following the mixer, an electrical band-pass filter (BPF) with a 3-dB passband between 24.5 GHz and 29.5 GHz, as shown in Fig. 5(b), is employed to remove the mirrored signal appearing at lower sideband. The BPFs at both the Tx side and the Rx side are customized yet low-cost components. The RF signal is further amplified by SHF S807 B (23-dB gain, >55-GHz bandwidth, and 16-dBm P1dB). For the digital signals, the NRZ and the PAM-4 signal are generated by a low-cost DAC (SHF 613A, 3-bit resolution) with only 1 or 2 bits enabled, respectively, and amplified by SHF 806 E (26-dB gain, 42-GHz bandwidth, and >18-dBm P1dB). 16-dB attenuation is applied to the digital signals, therefore the overall gain is 10 dB. The digital signal and the RF signal are then combined as a digital-analog hybrid signal by three types of optional transmitter structures. For the single-drive MZM and the DML-based structure, the combination is realized by an electrical coupler. While for the IQ modulator-based structure, two signals are respectively loaded onto the I and Q branch via the sub-MZMs, with each biased at quadrature point $V_\pi/2$. Both branches contain optical carrier, and by tuning the phase shifter in the IQ modulator to reach the maximum output power, the digital and RF-modulated signals are combined optically. The DML used in the experiment works at 1550 nm with an output power of 7.5 dBm. In the structures based on the single-drive MZM and the

This article has been accepted for publication in a future issue of this journal, but has not been fully edited. Content may change prior to final publication. Citation information: DOI 10.1109/JLT.2020.3034381, Journal of Lightwave Technology



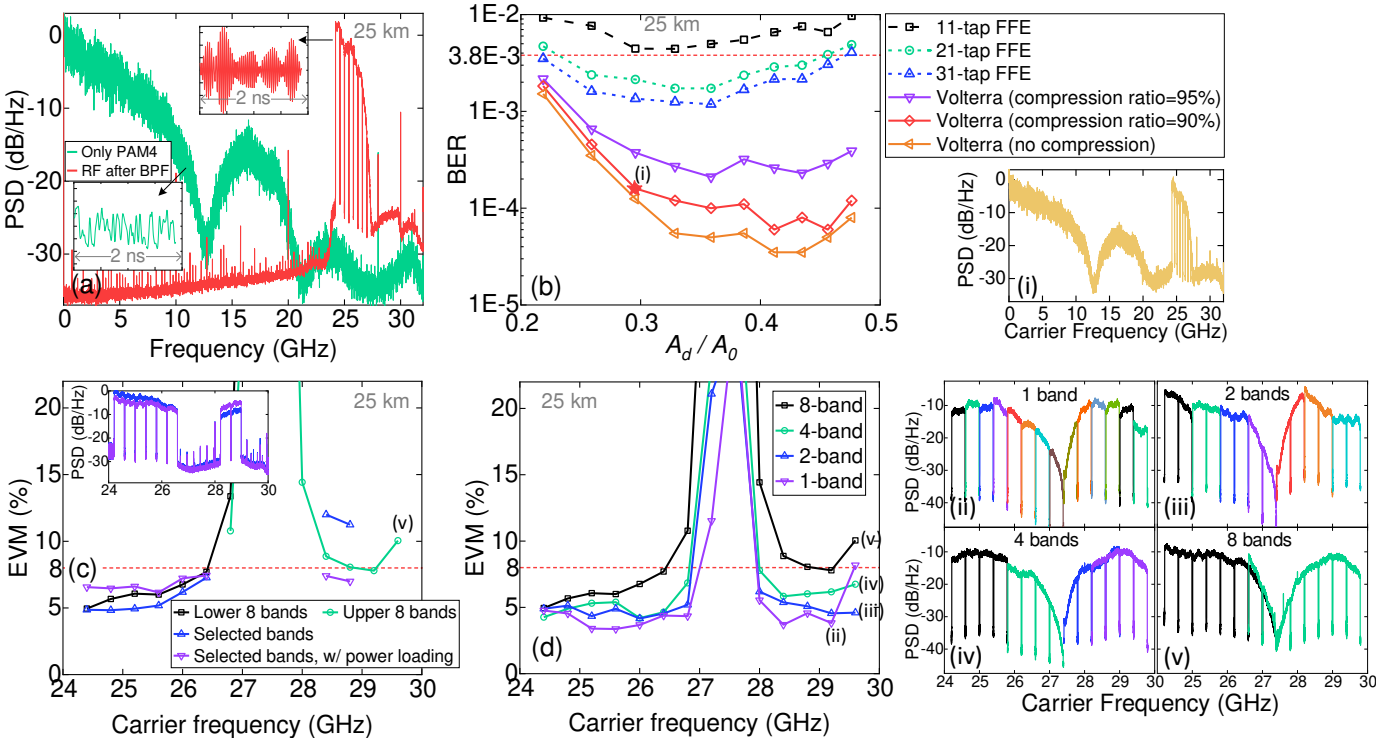


Fig. 6. (a) PD-detected spectra of the only-RF and only-PAM-4 signals over 25-km fiber, (b) BER of PAM-4 signal versus hybrid ratio, (c) comparison among different band selections for the 8×400-MHz RF signal in terms of EVM performance, (d) EVM performance of the 1, 2, 4, and 8×400-MHz RF signal. (i) Spectrum of the digital-analog hybrid signal, (ii)-(v): Spectra of the received IF signals aligned at corresponding RF bands. Results are measured with the SD-MZM-based setup.

IQ modulator, an external cavity laser (ECL) with <100-kHz linewidth and 15-dBm output power at 1550 nm is adopted in the experiment to ensure enough received optical power without optical amplifier and support a large-bandwidth RF signal. While in practical implementation, a distributed feedback (DFB) laser can be a more cost-effective alternative. After SSMF transmission, the optical signal is detected by a photodiode. The received electrical signal is split into two branches. One is fed to the first digital storage oscilloscope (DSO-1, Keysight DSO-Z 634A) with 160-GSa/s sampling rate and then re-sampled to 56 GSa/s for PAM-4 demodulation. Note that instead of filtering out the RF signal prior to equalization, the entire digital-analog hybrid signal is directly fed to the Volterra equalizer. Considering the interplay between the high-amplitude RF signal and the PAM-4 signal after fiber transmission, reserving the RF signal for the Volterra equalization will benefit the compensation of nonlinear distortion. The other branch is filtered by the electrical BPF and then mixed with the RF carrier for down-conversion. Finally, the obtained IF signal is sampled by DSO-2 (Keysight DSO91304A) with 20-GSa/s sampling rate, and processed by offline DSP.

### *B. Results based on single-drive MZM*

We first investigate the single-drive MZM based configuration and the performance after 25-km transmission is assessed. The first task is to find an appropriate hybrid ratio balancing the performance of the digital and RF signals. In this work, the hybrid ratio is optimized targeting the maximum number of RF bands. To find the best RF modulation depth

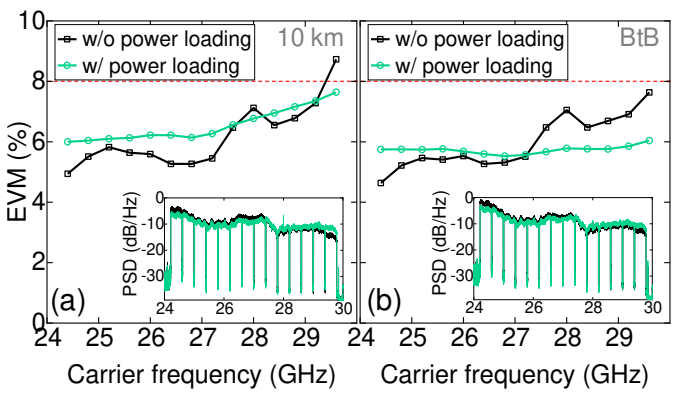


Fig. 7. EVM performance in (a) 10-km and (b) BtB cases. Results are measured with the SD-MZM-based setup.

without digital-to-analog crosstalk, we only apply an RF signal composed of 8 consecutive 400-MHz bands starting from 24.2 GHz. The received optical power (ROP) is set to 1 dBm, which is far below the PD saturation power. The received RF signal, as shown in Fig. 6(a), is directly sampled by DSO-1 to perform all-digital down-conversion and demodulation. Based on this hardware setup, the link nonlinearity mainly comes from the transmitter including the mixer, the driving amplifier, and the optical modulator, and the RF modulation depth is optimized in terms of the average EVM of all 8 bands. The changing of the hybrid ratio is further realized by controlling the output amplitude of DAC. The bit error rate (BER) of the PAM-4 signal with respect to the hybrid ratio is measured, as shown in Fig. 6(b). The adopted FFE is half-symbol-spaced, and the convergence of tap weights is based on least mean square (LMS)

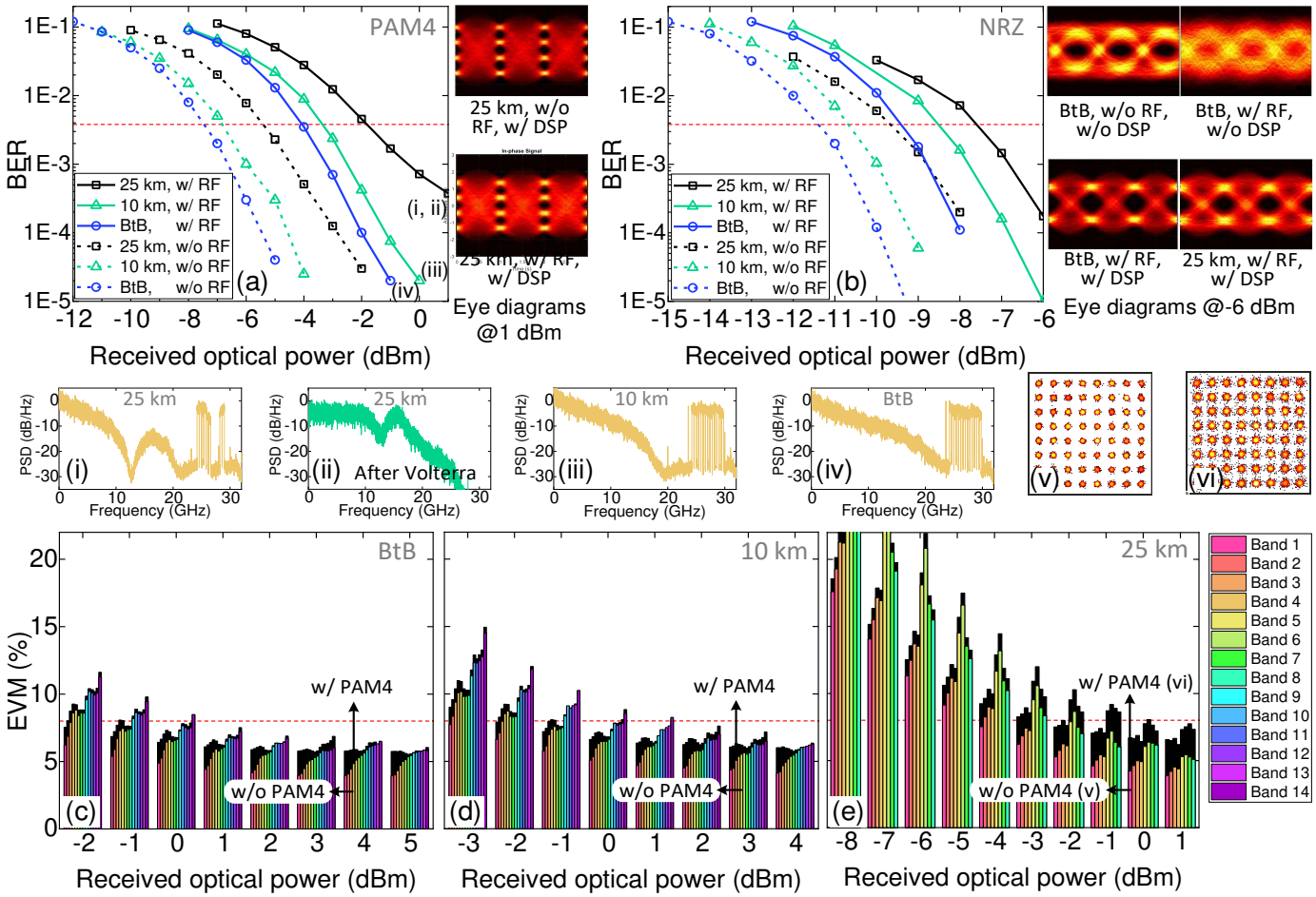


Fig. 8. BER versus received optical power for (a) the PAM-4 and (b) the NRZ signal, EVM versus received optical power via (c) 25-km, (d) 10-km, and (e) BtB transmission. (i)-(iv) Spectra of the digital-analog hybrid signals over different fiber lengths, (v)-(vi) constellation of RF band 1. Results are measured with the SD-MZM-based setup.

algorithm with a training length of $4\times10^3$ bits. 11, 21, and 31-tap lengths are tested, respectively. As the hybrid ratio $A_d/A_0$ increases from 0 to 0.3, the BER decreases. However, as the hybrid ratio grows beyond 0.35, the BER increases when using the FFE for the equalization, since a digital-analog hybrid signal with a large amplitude will experience significant nonlinearity and intensify the digital-analog crosstalk. Considering this issue, the Volterra nonlinear equalizer can significantly outperform FFE in a hybrid transmission system. In the experiment, a second-order half-symbol-spaced Volterra equalizer with 41-sample memory length is adopted. To lower the complexity, a sparse Volterra equalization is realized by pruning algorithm which forces the least significant weights to zero in training iterations, hence a large number of zero-weighted terms can be dropped out. The compression ratio is defined as the proportion of the pruned terms over the full unrepeated terms. Considering the hard-decision forward error correction (HD-FEC) threshold of $3.8\times10^{-3}$, power margin for the digital signal, the impairment of crosstalk, and the computational complexity, the hybrid ratio of 0.3 and the 90%-compressed Volterra equalizer are used in the MZM-based experiment.

The next step is to investigate how many mmW bands can be supported in the proposed structure. There are 14 mmW bands, each with 400-MHz bandwidth, in the frequency range of 24.2~29.8 GHz. We benchmark two groups of 8-band RF signals, with one group starting from 24.2 GHz and the other group starting from 26.6 GHz, as shown in inset (v) of Fig. 6. The RF carriers are tuned to 22.2 GHz and 24.6 GHz, respectively, and IF carriers start from 2.2 GHz in both groups. The measured EVM for the upper 8 bands and the lower 8 bands after the 25-km transmission is shown in Fig. 6(c). Note that the EVM of each band is calculated independently. The EVM result confirms that 8 consecutive bands cannot be supported simultaneously due to the dispersion-induced power fading. Instead, with 23.6-GHz RF carrier and IF carriers starting from 0.8 GHz, the specified bands consisting of band 1~6 and band 11, 12 are selected as the RF signal, as shown in the inset of Fig. 6 (c). Nevertheless, band 11 and 12 still cannot satisfy the EVM threshold for 64-QAM, since the IF signals for band 11 and 12 are at the edge of the mixer's bandwidth. To enable band 11 and band 12 for RF transmission, the power loading among RF bands is optimized, which pre-emphasizes each band with a constant inversely proportional to the specific band's overall EVM measured in the uniform power allocation situation. Using this technique, the EVM of all 8 bands after the 25-km transmission is below the 64-QAM threshold, and the CPRI-equivalent data rate for the 56-Gbps PAM-4 plus 8×400-MHz RF signals is ~186 Gbps. For reference, the EVM performance of the RF signals aggregating 1, 2, and 4 consecutive bands is

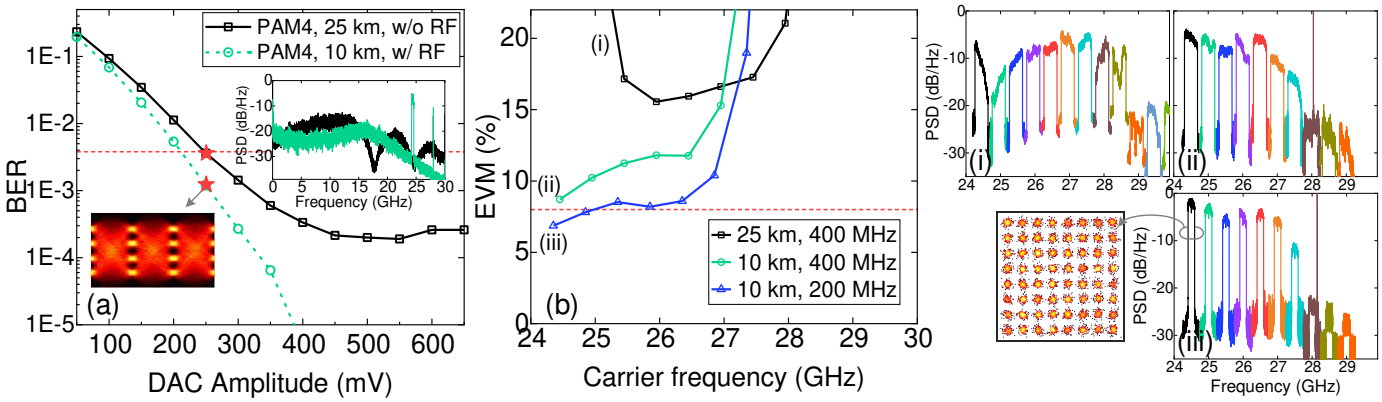


Fig. 9. (a) BER of the PAM-4 signal versus DAC output amplitude, (b) EVM performance of the one-band RF signal, DAC output is set to the minimum value satisfying HD-FEC in each case. (i)-(iii) Spectra of the received IF signals aligned at corresponding RF bands. Results are measured with the DML-based setup.

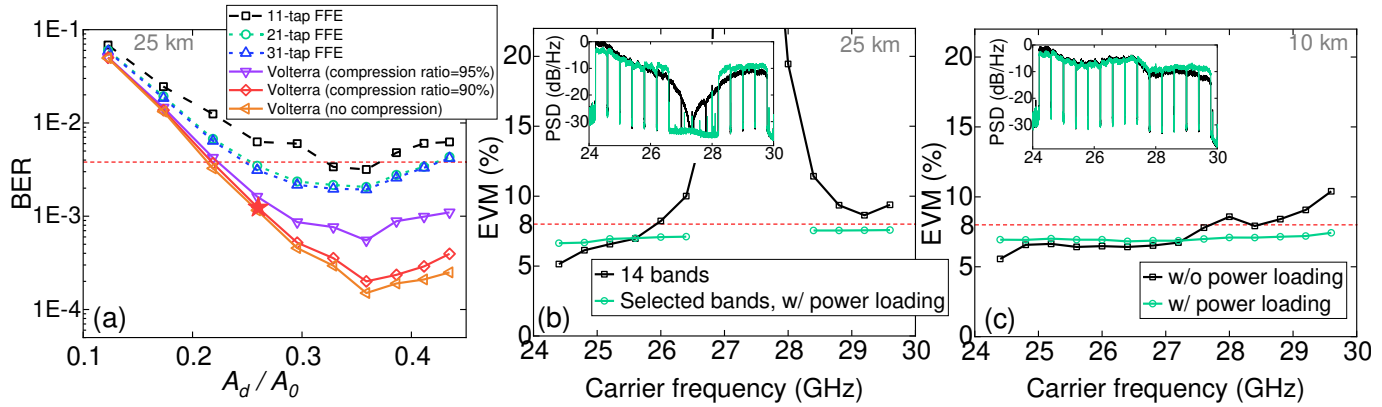


Fig. 10. (a) BER of the PAM-4 signal versus hybrid ratio, EVM of the RF signal over (b) 25-km and (c) 10-km transmission. Results are measured with the IQ-modulator-based setup.

also shown in Fig. 6(d). The spectra presented in Fig. 6 (ii)-(v) are the combination of the signal spectra received in different measurements, where the working bands of different measurements are distinguished by colors. As expected, better EVM can be achieved with fewer bands. The difference between 1-band and 2-band cases is very small since the system nonlinearity becomes the dominant limitation for a small number of bands. Similarly, band selection and power loading are also used for the back-to-back (BtB) case and the case after the 10-km transmission. Figure 7(a) and (b) show the EVM results of the 10-km case and the BtB case with a received optical power of 4 dBm and 5 dBm, respectively. Since there's no in-band dispersion-induced fading for these two cases, all the 14 bands can work simultaneously. It can be seen that the EVM performance degrades with the rising of the carrier frequency, which is mainly caused by the limited bandwidth of the optical modulator and RF components. The EVM at ~27 GHz is slightly better than the one at lower frequency since the frequency of ~27 GHz reaches the null of the digital signal and the digital-to-analog crosstalk at this frequency is much lower. Note that as shown in Fig. 7(a) and (b), the signal spectra of both the BtB and 10-km cases have a noticeable dip at 27.8 GHz, which is also observed in the following system setup. This dip is mainly caused by the imperfect response of the RF mixer. As a result, even the exact frequency null is at 28 GHz, the RF signal cannot reach the optimal performance at ~28 GHz.

With the above configurations of band selections and power loading, the BER performance of the PAM-4 and NRZ signals is given in Fig. 8(a) and (b) respectively. For comparison, the BER of the digital signal without superimposing the RF signal is also measured. In this case, the output amplitude of the DAC is maximized to increase the modulation depth. The peak-to-peak voltages of the DAC are 448 mV and 648 mV for generating the NRZ signal and the PAM-4 signal, respectively. The BER results show that the power penalty caused by the integration with RF signal is ~3 dB for the PAM-4 signal and ~2 dB for the NRZ signal. Inset (i), (iii), and (iv) of Fig. 8 show the electrical spectra after the PD detection, and inset (ii) shows the spectrum after the Volterra equalization, where it can be seen that the RF signal has been effectively eliminated. Note that to improve the receiver sensitivity and meet the power budget of the future-proofed PON system, an alternative avalanche photodiode (APD) or a semiconductor optical amplifier (SOA) could be applied. Besides, in a real deployment, the RF signal bandwidth can be narrower than the one in this setup, hence the hybrid ratio should be increased to reduce the power penalty of the digital signal.

Figure 8 (c)-(e) show the EVM performance of the RF signal as a function of the received optical power. The bright column represents the EVM of the RF signal without superimposing the PAM-4 signal, and the full column including the dark portion represents the result with superimposition. Considering the 25-km case, the EVM of all 8 bands is below the 64-QAM threshold with a received optical power of 1 dBm or -1 dBm for the case of with or without superimposing the PAM-4 signal, respectively. Therefore, the superimposition of the PAM-4

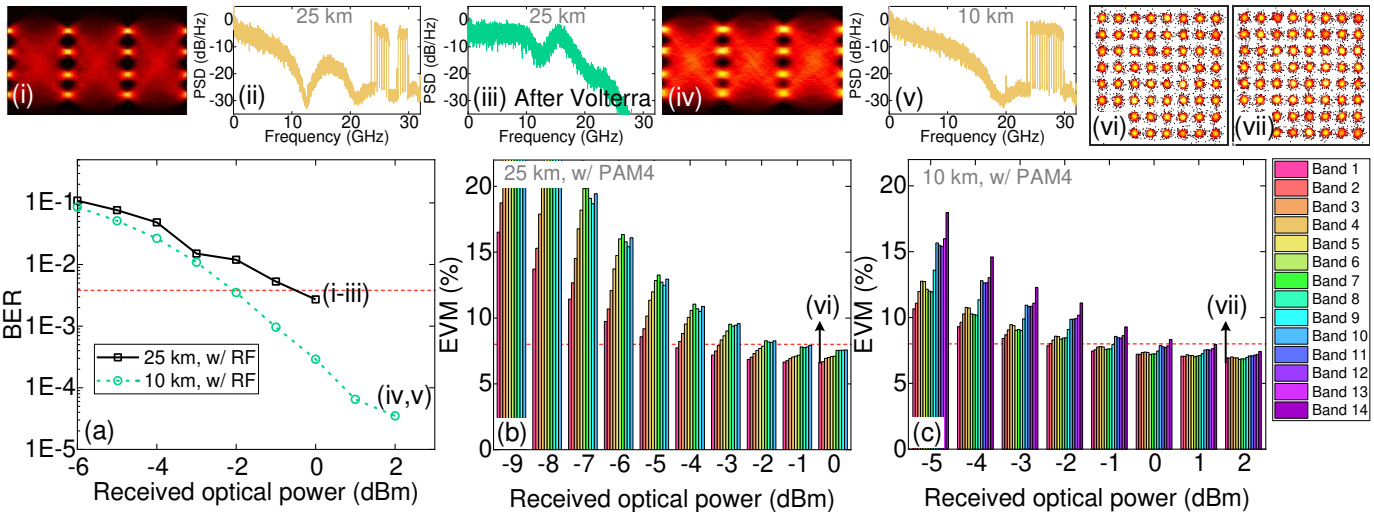


Fig. 11. (a) BER of the PAM-4 signal versus received optical power, EVM of the RF signal versus received optical power over (b) 25-km and (c) 10-km transmission. (i), (iv) eye diagrams, (ii), (iii), and (v) spectra of the digital-analog hybrid signals over different fiber lengths, (vi)-(vii) constellation of RF band 1. Results are measured with the IQ-modulator-based setup.

signal introduces a 2-dB power penalty. For the BtB and the 10-km cases, the EVM of all 14 bands is below the 64-QAM threshold with a received optical power of 1 dBm and 2 dBm respectively, regardless of whether superimposing the PAM-4 signal. It can be seen that the low-frequency bands perform better without superimposing the PAM-4 signal, especially when the received optical power is high and the digital-to-analog crosstalk is the dominant limiting factor. For a low received optical power, the impact of superimposing the PAM-4 signal is less since the OSNR starts to play a dominant role.

### C. *Results based on DML*

Secondly, we investigate the SNF scheme in the DML-based system. Compared to external modulation, direct modulation usually has a lower OSNR, narrower bandwidth, and stronger chirp effect. In order to reduce the digital-to-analog crosstalk for the RF signal, we try to decrease the modulation depth of the PAM-4 signal. With the RF signal turned off, Fig. 9(a) shows the BER performance of the PAM-4 signal with respect to the driving amplitude of the DAC, where the 250-mV amplitude is the minimum to meet the BER threshold. With this DAC amplitude, an RF signal with one 400-MHz band is applied and Fig. 9(b) shows its EVM performance. By fixing the IF carrier at 3.2 GHz and tuning the RF carrier, the EVM of the RF signal is measured across the 24.2~29.8-GHz span. Fig. 9 inset (i) shows the combination of signal spectra extracted from different measurements. Nevertheless, the results can never satisfy the 64-QAM threshold at any band after 10-km or 25-km transmission, even if the amplitude of the RF signal is optimal. The primary limitation of the DML-based RoF link is the interplay between the chirp of DML and the CD of fiber, which interferes with the RF signal [28]. In this case, the distance of the DML-based hybrid transmission system is restricted. Besides, given the 3-dB bandwidth of the DML is ~21 GHz, the power fading at mmW band is another issue. In a real system, a high-gain driver can be applied to boost the RF power before launching into an antenna, in order to compensate for the RF attenuation. To fulfill the 10-km hybrid transmission based on DML, the RF bandwidth is shrunk to 200 MHz, hence the PSD of RF signal is increased and the EVM threshold for 64-QAM is satisfied at the bands of 24~25 GHz, as shown in Fig. 9(b).

### D. *Results based on IQ modulator*

Finally, we investigate the SNF scheme in the IQ-modulator-based system. Similar to the single-drive-MZM-based system, the AWG output amplitude is configured with the optimal value of ~0.9 V in order to prioritize the optimization of the RF signal. Then, the hybrid ratio $A_d/A_0$ is optimized according to the BER of the PAM-4 signal by varying the DAC output amplitude. The FFE with different numbers of taps and the Volterra equalizers are compared, as shown in Fig. 10(a). The Volterra equalizer with 90% compressed computation complexity can achieve a satisfying balance between performance and complexity, thus it is adopted in the following measurement. The DAC amplitude is set to 250 mV which is the minimum value satisfying the BER threshold. With this value, the hybrid ratio measured at IQ modulator electrical ports is ~0.26. The RF carrier and the first IF carrier are set to 23.6 GHz and 0.8 GHz, respectively. Fig. 10(b) shows the EVM performance of the RF signal after 25-km transmission at a received optical power of 0 dBm, with all the 14 consecutive bands in the frequency range of 24.2~29.8 GHz enabled. By selecting the best 10 bands and applying power loading, the EVM of all 10 bands can be below the 64-QAM threshold. The EVM performance of the RF signal after 10-km transmission at a received optical power of 2 dBm is shown in Fig. 10(c), where all the 14 consecutive bands satisfy the 64-QAM threshold with the help of power loading.

The BER of the PAM-4 signal is measured after 25-km and 10-km transmission with the RF signal superimposed, as illustrated in Fig. 11(a). The EVM of each band in the RF signal is measured as a function of the received optical power after 25-km and 10-km transmission, as shown in Fig. 11(b) and (c). Compared to the single-drive MZM based scheme, the IQ-modulator based scheme can support 2 more bands for the RF signal after 25-km transmission. As shown in Fig. 5(a), the bandwidth of the IQ modulator is even lower than the single-drive MZM, therefore the high-frequency attenuation acting on

the RF signal should be more severe for the IQ-modulator based scheme. However, the IQ modulator has the superiority of consisting of two sub-MZMs, which can be independently modulated with the digital and RF signals. Therefore, the modulation depth is not shared, resulting in less nonlinearity-induced crosstalk. On the other hand, the single-drive MZM based scheme is more cost-effective while still offering a large RF capacity.

## V. Conclusions

In this paper, we propose and demonstrate a bandwidth-efficient spectral-null-filling technology for digital-analog hybrid-optical access, where the future-proofed high-volume PAM-4/NRZ signal and the 5G mmW-band RF signal are converged in a gap-less way. The capacity of the RF signal is theoretically formulated. The PAM-4 signal is generated by a 2-bit DAC instead of a high-resolution one, and the Volterra nonlinear equalizer is used to remove the digital-analog crosstalk. Band selection and power loading are employed to address the CD-induced RF power fading. The proposed scheme is verified based on three types of modulators, i.e. MZM, DML, and for the first time, the IQ modulator with both branches biased at quadrature point. After 25-km transmission, the DML can only be used to converge the PAM-4 signal with one 200-MHz band due to the CD-chirp interplay, while the MZM and the IQ modulator can support 8× and 10×400-MHz bands, respectively. The SNF technology enables a digital-analog-orchestrated fronthaul interface and provides a cost-efficient solution for future high-capacity wired and wireless optical access networks.

## References


[1] D. Nesset, "PON roadmap," *IEEE/OSA J. Opt. Commun. Netw.*, vol. 9, no. 1, pp. A71–A76, Jan. 2017.

[2] I. A. Alimi, A. L. Teixeira, and P. P. Monteiro, "Toward an efficient C-RAN optical fronthaul for the future networks: a tutorial on technologies, requirements, challenges, and solutions," *IEEE Commun. Surveys Tuts.*, vol. 20, no. 1, pp. 708–769, Firstquarter 2017.

[3] Higher speed passive optical networks – Requirements, ITU-T Recommendation G.9804.1, 2019.

[4] V. Houtsma, D. V. Veen, and R. Bonk, "Options for Single wavelength 50G TDM-PON," IEEE 802.3ca, Sep. Meeting, houtsma_3ca_1_0917, Sep. 2017.

[5] J. Huang, and Y. Yuan, "White Paper of Next Generation Fronthaul Interface Version 1.0," China Mobile Research Institute Tech. Rep., Jun. 2015.

[6] A. D. L. Oliva, X. C. Perez, A. Azcorra, A. D. Giglio, F. Cavaliere, D. Tiegelbekkers, J. Lessmann, T. Haustein, A. Mourad, and P. Iovanna, "Xhaul: toward an integrated fronthaul/backhaul architecture in 5G networks," *IEEE Wireless Commun.*, vol. 22, no. 5, pp. 32–40, Oct. 2015.

[7] Common Public Radio Interface: eCPRI Interface Specification, eCPRI Specification V2.0, May 2019.

[8] 5G-Oriented OTN Technology White Paper, China Telecom. White Paper, Mar. 2017.

[9] L. Li, M. Bi, H. Xin, Y. Zhang, Y. Fu, X. Miao, and W. Hu, "Enabling Flexible Link Capacity for eCPRI-Based Fronthaul with Load-Adaptive Quantization Resolution," *IEEE Access*, vol. 7, pp. 102174–102185, Jul. 2019.

[10] M. A. Ali, G. Ellinas, H. Erkan, A. Hadjiantonis, and R. Dorsinville, "On the vision of complete fixed-mobile convergence," *J. Lightw. Technol.*, vol. 28, no. 16, pp. 2343–2357, Aug. 2010.

[11] S. Gosselin et al., "Fixed and Mobile Convergence: Which Role for Optical Networks?" *IEEE/OSA J. Opt. Commun. Netw.*, vol. 7, no. 11, pp. 1075–1083, 2015.

[12] G. Shen, R. S. Tucker, and C. J. Chae, "Fixed mobile convergence architectures for broadband access: Integration of EPON and WiMAX," *IEEE Commun. Mag.*, vol. 45, no. 8, pp. 44–50, Sep. 2007.

[13] B. Liu, X. Xin, L. Zhang, J. Yu, Q. Zhang, and C. Yu, "A WDM-OFDM-PON architecture with centralized lightwave and PolSK-modulated multicast overlay," *Opt. Exp.*, vol. 18, no. 3, pp. 2137–2143, Feb. 2010.

[14] Y. Kaneko, T. Higashino, and M. Okada, "An empirical performance evaluation of an interference suppression scheme for radio over fiber simultaneously transmitted with baseband on-off keying," in *Proc. Int. Symp. Commun. Inf. Technol.*, Nara, Japan, 2015, pp. 221–224.

[15] T. Shao, and J. Yao, "Millimeter-wave and UWB over a colorless WDM-PON based on polarization multiplexing using a polarization modulator," *J. Lightw. Technol.*, vol. 31, no. 16, pp. 2742–2751, Aug. 2013.

[16] A. Chowdhury, H. C. Chien, Y. T. Hsueh, and G. K. Chang, "Advanced system technologies and field demonstration for in-building optical-wireless network with integrated broadband services," *J. Lightw. Technol.*, vol. 27, no. 12, pp. 1920–1927, Jun. 2009.

[17] T. Shao, F. Paresys, Y. L. Guennec, G. Maury, N. Corrao, and B. Cabon, "Convergence of 60 GHz radio over fiber and WDM-PON using parallel phase modulation with a single Mach–Zehnder modulator," *J. Lightw. Technol.*, vol. 30, no. 17, pp. 2824–2831, Jun. 2012.

[18] C. Lim, and K. L. Lee, "Enabling technologies incorporating optical tandem single sideband for optical-wireless integrated access networks," *J. Lightw. Technol.*, vol. 28, no. 10, pp. 1496–1502, Mar. 2010.

[19] C. T. Lin, J. Chen, P. C. Peng, C. F. Peng, W. R. Peng, B. S. Chiou, and S. Chi, "Hybrid optical access network integrating fiber-to-the-home and radio-over-fiber systems," *IEEE Photon. Technol. Lett.*, vol. 19, no. 8, pp. 610–612, Mar. 2007.

[20] T. Kamisaka, T. Kuri, and K. I. Kitayama, "Simultaneous modulation and fiber-optic transmission of 10-Gb/s baseband and 60-GHz-band radio signals on a single wavelength," *IEEE Trans. Microw. Theory Tech.*, vol. 49, no.10, pp. 2013–2017, Oct. 2001.

[21] T. Ohtsuki, T. Aiba, and M. Matsuura, "Simultaneous Radio-Frequency and Baseband Signal Transmission Over a Multimode Fiber," *IEEE Photon. J.*, vol. 11, no. 6, pp. 1–12, Dec. 2019.

[22] C. Chen, M. J. Crisp, R. V. Penty, I. White, and M. Crisp, "Transmission of Simultaneous 10Gb/s Ethernet and Radio-over-Fiber Transmission using In-band Coding," in *Proc. Opt. Fiber Commun. Conf. Exhib.*, Anaheim, CA, USA, Paper OM3D.1, 2013.

[23] P. C. Peng, L. H. Yen, C. H. Chang, Y. C. Chen, and J. J. Jhang, "Hybrid wireline and wireless transport system based on polarization modulator," *IEEE Photon. Technol. Lett.*, vol. 25, no. 11, pp. 1069–1072, Apr. 2013.

[24] S. Yao, Y. W. Chen, S. J. Su, Y. Alfadhli, S. Shen, R. Zhang, and G. K. Chang, "Non-orthogonal uplink services through co-transport of D-RoF/A-RoF in mobile fronthaul," *J. Lightw. Technol.* , (to be published).

[25] C. Browning, A. Farhang, A. Saljoghei, N. Marchetti, V. Vujicic, L. E. Doyle, and L. P. Barry, "5G wireless and wired convergence in a passive optical network using UF-OFDM and GFDM," in *Proc. IEEE Int. Conf. Commun. Workshops*, Paris, France, pp. 386–392, 2017.

[26] User Equipment (UE) radio transmission and reception; Part 2: Range 2 Standalone (Release 16), 3GPP TS 38.101-2 V16.1.0, Sep. 2019.

[27] Common Public Radio Interface (CPRI); Interface Specification, CPRI Specification V7.0, CPRI, Oct. 2015.

[28] B. G. Kim, S. H. Bae, H. Kim, and Y. C. Chung, "RoF-Based Mobile Fronthaul Networks Implemented by Using DML and EML for 5G Wireless Communication Systems," *J. Lightw. Technol.*, vol. 36, no. 14, pp. 2874–2881, Jul. 2018.